Nonlinear Evolution and Persistence of Cellular Patterns in Self-Sustained Two-Dimensional Detonations

S. Roy Choudhury, 1 Hardeo M. Chin, 2 Sheikh Salauddin, 2 and Kareem A. Ahmed 2

(Dated: 29 July 2021)

A nonlinear theory for the development and persistence of cellular two-dimensional patterns behind the shock front in self-sustained detonations is developed. A recent, significantly simplified and carefully-validated, detonation model¹ is used as the basis for the analysis.

In the spirit of earlier investigations of a variety of hydrodynamic and hydromagnetic instabilities, crossed-field microwave sources, tokamak edge plasmas, and other areas, our first approach here replaces the actual numerically computed equilibrium profiles by box-shaped ones having a jump discontinuity. The results for both the shapes and dimensions of the persistent two-dimensional cells picked out by our nonlinear analysis agree well with those in 1 for the same sets of parameters. The only significant discrepancy is in the wavelength of the cellular patterns along the reaction channel.

Approximations of actual equilibrium profiles by step discontinuities, as done here, are most accurate for long-wavelength regimes where the waves essentially do not register the actual spatial profiles. Future work towards remedying the above discrepancy will be based on refined versions of the normal forms here, with coefficients which are integrals over the actual spatial equilibrium profiles.

I. INTRODUCTION

Detonations are supersonic combustion waves which involve complex interactions between chemical kinetics, turbulence, and compressibility. A brief, but quite comprehensive history of the identification of the phenomenon as a supersonic wave propagating at speeds several orders of magnitude higher than ordinary flames is given in¹. This includes early analyses of Mikhelson, Chapman and Jonguet, and of Zeldovich, von Neumann and Doering^{2,3} elucidating the requirement of having a shock wave that can compress the reacting gas to high enough temperatures to ignite chemical reactions behind the shock. The sonic waves created by the resulting heat release support both shock propagation and acceleration of the flow relative to the shock. Self-sustained detonations result if sufficiently large acceleration causes the flow relative to the shock to reach sonic conditions, with the sonic point behind the shock isolating the flow between that point and the shock from the influence of conditions further downstream of the shock. This isolated 'reaction zone' allows a self-sustained wave, which is seen in most detonations.

In the work of Zel'dovich, von Neumann and Doering², which also pertained to the blast waves accompanying atomic bomb explosions⁴ and is nowadays universally referred to as ZND theory, one-dimensional, steady state detonations were analyzed. However, early experiments^{2,3} already revealed the unsteady and complex dynamics and multidimensional nature of the phenomenon. An early review of the literature on stability analyses of the steady ZND solutions to explain such complex dynamics may be found in⁵. Stability analysis for the full model was found to be complicated, and notably includes the work in⁶ which used weakly nonlinear analysis based on an integrodifferential model to explain the formation of diamond-shaped cells in the reaction zone behind the shock, as well as summaries of earlier analyses using matched asymptotic expansions. Many years later, Lee and Stewart⁷

re-investigated the problem for an idealized model using the standard method of normal modes⁸.

As with many classical hydrodynamics instabilities⁸, applications of linear stability theory to the detonation problem⁹¹⁴ include detailed analyses of the eigenfunctions, the linear neutral curve, and analytical multimode solutions in the weakly unstable regime corresponding to the most unstable wavenumber(s)^{15,16} for steady detonations. Such standard weakly nonlinear analyses^{17,18} have also been employed^{12,1319–24} to treat a variety of phenomena, including further bifurcations to pulsating modes via limit cycle creation through Hopf bifurcation, possible combinations of fast and slow modes as the activation energy increases, mode selection, diamond-shaped cell formation behind the shock at the most linear unstable wavenumber, the spacing of such cells, and other related features.

Other treatments using sophisticated matched asymptotic expansions or boundary layer theory⁴¹ on simplified models include those of Rosales and Majda²⁵ and Majda²⁶.

Many of the above studies treated known features of gaseous detonation, such as unsteady oscillations in the lead shock velocity, formation of triple points behind the shock where additional transversely-propagating shocks in the very non-uniform flow there intersect with the lead shock, as well as the formation of fish-scale cellular structures^{2,3,27}. Theoretical prediction of the origin and structure of cellular two-dimensional detonation has proved more difficult, with limited progress resulting from the use of simplified models in various asymptotic regimes as reviewed in¹.

Given the above, Faria et al¹ developed a simplified asymptotic theory using a sophisticated asymptotic weakly nonlinear analysis. Their aim was to capture the complex bifurcation sequences seen in one-dimensional detonations, as well as the fish-scale cells observed in two-dimensional detonations. They built on the theory developed earlier in^{25,28} which, as with²⁶, were known to lack the necessary complexity in

¹⁾ Department of Mathematical Sciences, University of Central Florida.

²⁾Department of Mechanical and Aerospace Engineering, University of Central Florida

their reaction kinetics to reproduce the dynamics of real detonations. In particular, they carefully tested this simplified model against the corresponding results from the full reactive Euler model of detonations. For their simplified model and the full reactive Euler system, they compared: a. the linear stability spectrum of traveling wave solutions, b. numerical solutions and bifurcation sequences in the nonlinear regime of one-dimensional detonations, and c. numerical formation of cellular structures in two-dimensional detonations. Good agreement was found on all qualitative features, including fairly close quantitative agreement in many instances as well in the small heat release, large activation energy, and Newtonian limit in which they developed their simplified model.

In this paper, we will develop a weakly nonlinear analysis of cellular pattern formation and persistence in two-dimensional detonations based on this simplified and carefully-validated model in¹. In particular, our treatment reveals the persistence of weakly-nonlinear pulsating fish-scale patterns whose location, shape, and spatial extent agree well with the numerically obtained cells in 1 for the corresponding parameter values. In our treatment, for this first detailed approach to this problem, we bring in additional simplifications to the equilibrium profiles using ideas employed earlier in classical hydrodynamics stability analysis^{8,29}, tokamak edge plasmas³⁰, and the operational theory of high-power crossedfield microwave sources $^{31-34}$. Our results will be seen to agree with those obtained from numerical simulations in most aspects. The main discrepancy between our asymptotic treatment of cell formation and the numerical cells presented in 1 is in the cell wavenumber in the direction along the reaction channel or zone. Hence, at the very end, we also mention proposed future work in refining the results of this paper. That would require re-deriving the normal forms or nonlinear secularity conditions on which the results in this paper are based to more complex ones whose coefficients would involve integration over the exact equilibrium profiles³⁵_38 along the reaction channel.

The remainder of this paper is organized as follows. In Section II, we briefly recapitulate the simplified model developed using a sophisticated asymptotic analysis in¹. Section IIIA briefly reviews the exact equilibrium profiles in¹, while Section IIIB presents a simplified box-shaped model of these equilibrium profiles involving step discontinuities, as well as the motivation for using them and their possible regimes of validity. Section IV develops a multiple scales expansion of the variables in our model for the purposes of the nonlinear stability analysis, while Section V presents the linear stability analysis of the box equilibrium solutions. The analysis of the second-order solutions is contained in Section VI, while Section VII derives the third-order secularity conditions or normal form for the validity or uniformity of the original multiple scales expansion of our variables in Section IV. Section VIII presents an analysis of this normal form for three-mode solutions, including both phase-modulated and amplitudemodulated solutions, while Section IX repeats that analysis for two-mode solutions and shows that such two mode solutions may indeed be stable (for various parameter sets corresponding to numerically derived cell patterns in¹) and correspond to persistent pulsating fish-scale patterns which are compared to those in¹. Finally Section X discusses our results, and possible future refinements. Some of the longer intermediate results in the derivations are contained in Appendices A and B.

II. GOVERNING EQUATIONS

In this sub-section, we introduce the simplified governing model for self-sustained detonations. Its derivation from the two-dimensional reactive Euler equations using a simplified one-step Arrhenius kinetics, together with detailed numerical comparisons to the full starting model, may be found in 1. The final asymptotic model for weakly nonlinear detonations derived in 1 consists of the forced set of transonic equations

$$\frac{\partial u}{\partial t} + u \frac{\partial u}{\partial x} + \frac{\partial v}{\partial y} = -\frac{\partial \lambda}{2\partial x} + v \frac{\partial^2 u}{\partial x^2}$$
 (1)

$$\frac{\partial v}{\partial x} = \frac{\partial u}{\partial y},\tag{2}$$

$$\frac{\partial \lambda}{\partial x} = -k(1 - \lambda) exp[\theta(\sqrt{q}u)]. \tag{3}$$

In these equations, p, u, v, ρ , and e denote pressure, horizontal velocity, vertical velocity, density, and energy per unit mass, respectively. We use λ as the reaction progress variable that takes values in the range $0 \le \lambda \le 1$ as the reactants ($\lambda = 1$) progress to the products ($\lambda = 0$). The other parameters v, v, v, v and v represent the rescaled dimensionless viscosity, pre-exponential factor, activation energy, and heat release respectively.

For the inviscid case, these are supplemented by the Rankine-Hugoniot (RH) conditions across the shock where the detonation occurs. For a flame propagating in the x-direction, defining the shock locus by $\phi(x,y,t) = x - s(y,t)$, and denoting the jump in any variable z by [z], the RH conditions simplify to¹:

$$s_{\tau} - [u^2]/2 + s_y[v] = 0$$
 (4)

$$s_{v}[u] + [v] = 0$$
 (5)

$$[\lambda] = 0 \tag{6}$$

III. EQUILIBRIUM SOLUTIONS

Considering traveling wave solutions $\bar{u} = \bar{u}(x - \bar{D}t)$ launched uniformly across the cross-section of the channel, and propagating along the length of the channel at speed \bar{D} , with the overbar denoting steady state values of all variables, yields

$$\bar{u} = \bar{D} + \sqrt{\bar{D}^2 - \bar{\lambda}} \tag{7}$$

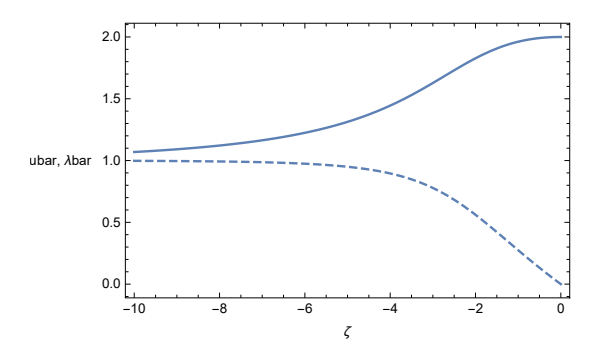


FIG. 1. Steady Profiles satisfying the correct boundary conditions for $\bar{D} = 1$. Dashed lines represent $\bar{\lambda}$, while \bar{u} is in solid lines.

with

$$\bar{\lambda}_{\zeta} = -k(1 - \bar{\lambda}) exp[\theta(\sqrt{q}\bar{u} + q\bar{\lambda})]$$
 (8)

and the traveling wave variable $\zeta = (x - \bar{D}t)$. The requirement that the solution for \bar{u} be real at the end of the reaction zone where $\bar{\lambda}$ takes its maximum value of unity leads to the restriction $\bar{D} \geq 1$, with the actual value of \bar{D} determined by the degree of overdrive. As in¹, our main focus in this paper will be on the important case of a self-sustained detonation setting in, where the steady state has a sonic point or shock at the end of the reaction zone located at $x = -\infty$ (the reaction zone is located behind the shock, i.e. x < 0).

Just behind the leading shock at x = 0 the reaction is complete and hence

$$\bar{\lambda}(0) = 0, \bar{u}(0) = 2\bar{D}.\tag{9}$$

with the second equation following from (7). At the opposite extremeity of the reaction zone, the end of the reaction zone, we have only reactants, and hence

$$\bar{\lambda}(-\infty) = 1, \bar{u}(-\infty) = \bar{D} + \sqrt{\bar{D}^2 - 1}, \tag{10}$$

Note that $\bar{D}=1$ for self-sustained detonations with a sonic point at the end of the reaction zone at $x=-\infty$, and thus $\bar{u}(-\infty)=\bar{D}$ for this case. This is the case investigated in this paper.

Plugging (7) into (8) and integrating the resulting first-order differential equation starting with the boundary conditions (9) yields the spatially inhomogeneous x-dependent profiles for $\bar{\lambda}$ (it is easiest to define a new variable $z=-\zeta$ and integrate forward in z. The boundary conditions (10) at the other end $\zeta=-\infty$ are automatically satisfied as (7) has already been incorporated into our differential equation. The corresponding profile for \bar{u} is then obtained from (7).

For the sake of completeness, we reproduce one such steady state profile for $\bar{D} = 1$ in Figure 1.

Note also that steady-state profiles such as these obtained from the simplified asymptotic model equations(1)-(3) have been quantitatively tested against ZND solutions of the reactive Euler equations in¹. They are generally found to agree well, to within five percentage deviation from the ZND profiles for realistic parameter values.

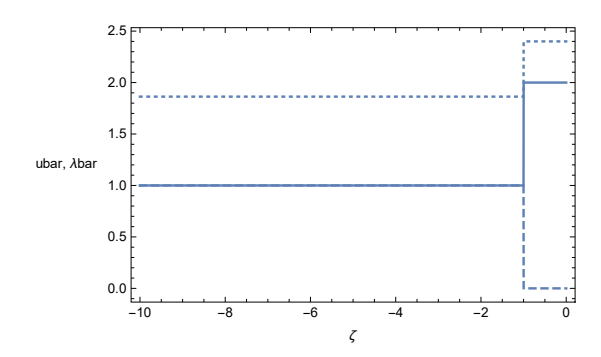


FIG. 2. Box Profiles satisfying the correct boundary conditions. Dashed lines represent $\bar{\lambda}$, while \bar{u} is in solid lines (for $\bar{D}=1$) and dotted lines (for $\bar{D}=1.2$).

A. Box Equlibrium Profiles

As mentioned in Section 1, our primary focus in this paper will be the weakly nonlinear evolution and nonlinear stability analysis to derive the saturated states resulting behind the shock. The linear stability analysis which has been detailed in 1 involves Weyl-type radiation boundary conditions at the end of the reaction zone as $x \to -\infty$ (see also 29 for further details on the treatment of such boundary conditions).

While nonlinear stability analysis of the spatially exact nonuniform equilibrium solutions derived above is analytically possible 33-35,37, we include a more analytically tractable approximate equilibrium in this subsection for our first approach to this problem in this paper. In this, we follow the practice of using simplified or mock-up equilibria in earlier work in many areas such as classical hydrodynamics stability analysis 8,29, tokamak edge plasmas 30, and the operational theory of highpower crossed-field microwave sources 31-34.

The linear eigenspectrum obtained using these approximate box profiles will be discussed subsequently, and found to agree quite well with the exact eigenvalues using the correct inhomogeneous steady state profile derived in the previous subsection. Note that similar approximate equilibrium profiles have shown good agreement in the nonlinear analysis of various hydrodynamic and magnetohydrodynamic instabilities in long-wavelength regimes²⁹ or crossed-field amplifiers³⁴ where the waves are longer than the spatial scale of the exact equilibrium profiles. In a similar spirit, we introduce the box equilibrium profiles for \bar{u} and $\bar{\lambda}$ shown in Figure 2. They are defined by the step function profiles:

$$\bar{u} = \begin{cases} \bar{D}, & x < -x_{step} \\ 2\bar{D}, & -x_{step} < x \le 0 \end{cases}$$
 (11)

$$\bar{\lambda} = \left\{ \begin{array}{ll} \bar{D}^2, & x < -x_{step} \\ 0, & -x_{step} < x \le 0 \end{array} \right\},\tag{12}$$

and satisfy the correct boundary conditions (9) and (10) at the two ends of the reaction zone.

Note that we have left the location $-x_{step}$ of the step jumps in these box-shaped profiles arbitrary. We consider this further later in the paper, as well as the required jump conditions across this discontinuity. In particular, we shall find that,

while the discontinuity ensures the correct values of the equilibrium variables at both ends of the reaction zone, it's actual location will not affect the nonlinear cell formation which will be our primary focus in this paper.

IV. MULTIPLE SCALES EXPANSION FOR NONLINEAR STABILITY ANALYSIS

In this section, we begin the stability analysis of the equilbria $\bar{u}(x)$ and $\bar{\lambda}(x)$ derived in the previous section. Note that the linear stability analysis using the exact equilibria in Figure 1 has been detailed in 1. We will briefly summarize that analysis in the next section, and compare it to the results obtained using the approximate box-shaped profiles of Figure 2 before proceeding to the nonlinear analysis in the subsequent sections.

The expansions around the equilibria take the form:

$$u = \bar{u}(x) + \varepsilon u_1(x, y, T_0, T_1, T_2) + \varepsilon^2 u_2(x, y, T_0, T_1, T_2) + \varepsilon^3 u_3(x, y, T_0, T_1, T_2)$$

$$v = \bar{v}(x) + \varepsilon v_1(x, y, T_0, T_1, T_2) + \varepsilon^2 v_2(x, y, T_0, T_1, T_2) + \varepsilon^3 v_3(x, y, T_0, T_1, T_2)$$
(13)

$$\lambda = \bar{\lambda}(x) + \varepsilon \lambda_1(x, y, T_0, T_1, T_2) + \varepsilon^2 \lambda_2(x, y, T_0, T_1, T_2) + \varepsilon^3 \lambda_3(x, y, T_0, T_1, T_2)$$

Introducing slow time scales T_i in the standard way

$$T_1 = \varepsilon t$$

$$T_2 = \varepsilon^2 t$$

$$T_3 = \varepsilon^3 t$$

utilizing the chain rule, the temporal derivatives become:

$$\frac{\partial}{\partial t} = \partial_t + \varepsilon \partial_{T_1} + \varepsilon^2 \partial_{T_2} + \varepsilon^3 \partial_{T_3} + \dots$$
 (14)

Using Eqns. (13) - (15) in Eqn. (1)-(3) yields equations at $\mathcal{O}(\varepsilon)$, $\mathcal{O}(\varepsilon^2)$, $\mathcal{O}(\varepsilon^3)$, which are contained in Appendix A.

Using the relation among \bar{U} , \bar{V} , $\bar{\lambda}$ the structure of the equations (A.1)-(A.3)(will change) at $\mathcal{O}(\varepsilon^i)$ may be written in the form:

$$-S_{i1}(x, y, T_{0}, T_{1}, T_{2}) + u_{i}(x, y, T_{0}, T_{1}, T_{2})\bar{u}'(x)$$

$$+ \frac{\partial u_{i}}{\partial T_{2}}(x, y, T_{0}, T_{1}, T_{2}) + \frac{\partial v_{i}}{\partial T_{0}}(x, y, T_{0}, T_{1}, T_{2})$$

$$+ \frac{1}{2} \frac{\partial \lambda_{i}}{\partial T_{0}}(x, y, T_{0}, T_{1}, T_{2}) - \bar{D} \frac{\partial u_{i}}{\partial T_{0}}(x, y, T_{0}, T_{1}, T_{2})$$

$$+ \bar{u}(x) \frac{\partial u_{i}}{\partial T_{0}}(x, y, T_{0}, T_{1}, T_{2}) \quad (15)$$

$$-S_{i2}(x, y, T_{0}, T_{1}, T_{2}) + \frac{\partial u_{i}}{\partial T_{1}}(x, y, T_{0}, T_{1}, T_{2})$$

$$- \frac{\partial v_{i}}{\partial T_{0}}(x, y, T_{0}, T_{1}, T_{2}) \quad (16)$$

$$-e^{\theta(q\bar{\lambda}(x)+\sqrt{q}\bar{u}(x)}k\lambda_{i}(x,y,T_{0},T_{1},T_{2}) - S_{i3}(x,y,T_{0},T_{1},T_{2}) +e^{\theta(q\bar{\lambda}(x)+\sqrt{q}\bar{u}(x)}k\theta(1-\lambda\bar{(}x)(q\lambda_{i}(x,y,T_{0},T_{1},T_{2}) +\sqrt{q}u_{i}(x,y,T_{0},T_{1},T_{2}) + \frac{\partial\lambda_{i}}{\partial T_{0}}(x,y,T_{0},T_{1},T_{2})$$
(17)

where the sources S_{ij} at $O(\varepsilon^i)$ in the j-th equation are given in Appendix A. By solving (9) for u_i and plugging the result in (8), the resulting equation can be solved for v_i . Solving (15) for $v_{i,y}$ and enforcing $v_{i,xy} = v_{i,yx}$ yields the generalized composite L operator and composite source Γ_i satisfying the equation:

$$L(\lambda_i) = \Gamma_i, \tag{18}$$

where

$$L(\lambda_{i}) = 2e^{k_{1}\sqrt{q}\theta + k_{2}q\theta}k(1 + (-1 + k_{2})q\theta)\frac{\partial^{2}\lambda_{i}}{\partial y^{2}} + 2e^{k_{1}\sqrt{q}\theta + k_{2}q\theta}k\frac{\partial^{2}\lambda_{i}}{\partial x\partial T_{0}} - 2e^{k_{1}\sqrt{q}\theta + k_{2}q\theta}kq\theta\frac{\partial^{2}\lambda_{i}}{\partial x\partial T_{0}} + 2e^{k_{1}\sqrt{q}\theta + k_{2}q\theta}kk_{2}q\theta\frac{\partial^{2}\lambda_{i}}{\partial x\partial T_{0}} - 2e^{k_{1}\sqrt{q}\theta + k_{2}q\theta}kq\theta\frac{\partial^{2}\lambda_{i}}{\partial x\partial T_{0}} + 2e^{k_{1}\sqrt{q}\theta + k_{2}q\theta}kk_{2}q\theta\frac{\partial^{2}\lambda_{i}}{\partial x\partial T_{0}} - 2e^{k_{1}\sqrt{q}\theta + k_{2}q\theta}kq\theta\frac{\partial^{2}\lambda_{i}}{\partial x^{2}} - 2\bar{D}e^{k_{1}\sqrt{q}\theta + k_{2}q\theta}k\sqrt{q}\theta\frac{\partial^{2}\lambda_{i}}{\partial x^{2}} - e^{k_{1}\sqrt{q}\theta + k_{2}q\theta}kk_{2}\sqrt{q}\theta\frac{\partial^{2}\lambda_{i}}{\partial x^{2}} + 2e^{k_{1}\sqrt{q}\theta + k_{2}q\theta}kk_{2}q\theta\frac{\partial^{2}\lambda_{i}}{\partial x^{2}} - 2\bar{D}e^{k_{1}\sqrt{q}\theta + k_{2}q\theta}kk_{2}q\theta\frac{\partial^{2}\lambda_{i}}{\partial x^{2}} + 2e^{k_{1}\sqrt{q}\theta + k_{2}q\theta}kk_{1}k_{2}q\theta\frac{\partial^{2}\lambda_{i}}{\partial x^{2}} - 2\bar{D}e^{k_{1}\sqrt{q}\theta + k_{2}q\theta}kk_{2}q\theta\frac{\partial^{2}\lambda_{i}}{\partial x^{2}} + 2e^{k_{1}\sqrt{q}\theta + k_{2}q\theta}kk_{1}k_{2}q\theta\frac{\partial^{2}\lambda_{i}}{\partial x^{2}} - 2\bar{D}e^{k_{1}\sqrt{q}\theta + k_{2}q\theta}kk_{2}q\theta\frac{\partial^{2}\lambda_{i}}{\partial x^{2}} + 2e^{k_{1}\sqrt{q}\theta + k_{2}q\theta}kk_{1}k_{2}q\theta\frac{\partial^{2}\lambda_{i}}{\partial x^{2}} - 2\bar{D}e^{k_{1}\sqrt{q}\theta + k_{2}q\theta}kk_{2}q\theta\frac{\partial^{2}\lambda_{i}}{\partial x^{2}} + 2e^{k_{1}\sqrt{q}\theta + k_{2}q\theta}kk_{1}k_{2}q\theta\frac{\partial^{2}\lambda_{i}}{\partial x^{2}} - 2\bar{D}e^{k_{1}\sqrt{q}\theta + k_{2}q\theta}kk_{2}q\theta\frac{\partial^{2}\lambda_{i}}{\partial x^{2}} + 2e^{k_{1}\sqrt{q}\theta + k_{2}q\theta}kk_{1}k_{2}q\theta\frac{\partial^{2}\lambda_{i}}{\partial x^{2}} - 2\bar{D}e^{k_{1}\sqrt{q}\theta + k_{2}q\theta}kk_{2}q\theta\frac{\partial^{2}\lambda_{i}}{\partial x^{2}} + 2e^{k_{1}\sqrt{q}\theta + k_{2}q\theta}kk_{1}k_{2}q\theta\frac{\partial^{2}\lambda_{i}}{\partial x^{2}} - 2\bar{D}e^{k_{1}\sqrt{q}\theta + k_{2}q\theta}kk_{2}q\theta\frac{\partial^{2}\lambda_{i}}{\partial x^{2}} + 2e^{k_{1}\sqrt{q}\theta + k_{2}q\theta}kk_{1}k_{2}q\theta\frac{\partial^{2}\lambda_{i}}{\partial x^{2}} - 2\bar{D}e^{k_{1}\sqrt{q}\theta + k_{2}q\theta}kk_{2}q\theta\frac{\partial^{2}\lambda_{i}}{\partial x^{2}} + 2e^{k_{1}\sqrt{q}\theta + k_{2}q\theta}kk_{1}k_{2}q\theta\frac{\partial^{2}\lambda_{i}}{\partial x^{2}} - 2\bar{D}e^{k_{1}\sqrt{q}\theta + k_{2}q\theta}kk_{2}q\theta\frac{\partial^{2}\lambda_{i}}{\partial x^{2}} + 2e^{k_{1}\sqrt{q}\theta + k_{2}q\theta}kk_{1}k_{2}q\theta\frac{\partial^{2}\lambda_{i}}{\partial x^{2}} - 2\bar{D}e^{k_{1}\sqrt{q}\theta + k_{2}q\theta}kk_{2}q\theta\frac{\partial^{2}\lambda_{i}}{\partial x^{2}} - 2\bar{D}e^{$$

$$\Gamma_{i} = -2\left(e^{k_{1}\sqrt{q}\theta + k_{2}q\theta}k(-1 + k_{2})\sqrt{q}\theta\frac{\partial S_{i2}}{\partial y} + \frac{\partial^{2}S_{i3}}{\partial y^{2}} - e^{k_{1}\sqrt{q}\theta + k_{2}q\theta}k\sqrt{g}\theta\frac{\partial S_{i1}}{\partial y} + e^{k_{1}\sqrt{q}\theta + k_{2}q\theta}kk_{2}\sqrt{q}\theta\frac{\partial S_{i1}}{\partial y} + \frac{\partial^{2}S_{i3}}{\partial x\partial T_{0}} - \bar{D}\frac{\partial^{2}S_{i3}}{\partial x^{2}} + k_{1}\frac{\partial^{2}S_{i3}}{\partial x^{2}}\right)$$
(20)

V. LINEAR STABILITY ANALYSIS

In this section, we consider the stability analysis for the linear or $O(\varepsilon)$ perturbation or field variables.

A. Linear solutions for Exact Equilibria

In the first subsection, we briefly recapitulate the results of the linear stability analysis of 1 in our notation. As is standard in the method of normal modes 8 , Faria et al 1 considered one arbitrary Fourier mode or wavenumber k_{y} in the y-direction, and subsequently focused on the most unstable mode which first undergoes linear instability. Hence, assuming linear variables of the form

$$u_1(x, y, T_0, T_1, T_2) = u_1(x, T_1, T_2) e^{\sigma T_0 + ik_y} + u_{10} * (x, T_1, T_2) e^{\sigma T_0 - ik_y y}$$
(21)

$$v_1(x, y, T_0, T_1, T_2) = v_{10}(x, T_1, T_2) e^{\sigma T_0 + ik_y y} + v_{10} * (x, T_1, T_2) e^{\sigma T_0 - ik_y y}$$
(22)

$$\lambda_1(x, y, T_0, T_1, T_2) = \lambda_1(x, T_1, T_2) e^{\sigma T_0 + ik_y} + \lambda_{10} * (x, T_1, T_2) e^{\sigma T_0 - ik_y y}$$
(23)

where the * denotes a complex conjugate. Using these in (1)-(3) yields the equations for the linear field variables:

$$(\bar{u} - \bar{D})u_1' = -(\sigma + \bar{u}')u_1 + \sigma\bar{u}' -ik_yv_1 - [g(x)u_1 + h(x)\lambda_1]/2$$
 (24)

$$v_1' = ik_y u_1 - ik_y \bar{u}', \qquad (25)$$

$$\lambda_1' = g(x)u_1 + h(x)\lambda_1 \tag{26}$$

where

$$g(x) = -k\theta q^{1/2} (1 - \bar{\lambda}) exp \left[\theta(q^{1/2}\bar{u} + q\bar{\lambda}) \right], \quad (27)$$

and

$$h(x) = -k \left[\theta q (1 - \bar{\lambda}) - 1 \right] exp \left[\theta (q^{1/2} \bar{u} + q \bar{\lambda}) \right]. \tag{28}$$

These are the explicit version of the $O(\varepsilon)$ equations in Appendix A after substituting the linear fields (21)-(23).

Using (24)-(26), the composite equation (18) at $O(\varepsilon)$ simplifies to

$$\left[(\bar{u} - \bar{D}) \left(\frac{\lambda_1' - \lambda_1 h(x)}{g(x)} \right)' + \left(\sigma + \bar{u}' + g(x)/2 \right) \right) \left(\frac{\lambda_1' - \lambda_1 h(x)}{g(x)} \right) \\
- \bar{u}' + h(x)\lambda_1/2' = \frac{k_y^2}{\sigma} \left[\sigma \left(\frac{\lambda_1' - \lambda_1 h(x)}{g(x)} \right) - \bar{u}' \right] \quad (29)$$

Also, using (24)-(26) in the Rankine-Hugoniot conditions (4)-(6), the boundary conditions¹ on the linear fields at the shock location x = 0 are:

$$u_1(0) = 2\sigma, v_1(0) = -2ik_v\bar{D}, \lambda_1(0) = 0$$
 (30)

Using these in (24)-(26), as well as in the *x*-derivative of (26) yields the corresponding boundary conditions for the composite third-order equation (??) for the first-order variable λ_1

$$\lambda_1(0) = 0, \lambda_1'(0) = 2\sigma g(0),$$
 (31)

$$\lambda_1''(0) = 2\sigma g'(0) + g(0) \left[-2\sigma^2 - \sigma \bar{u}'(0) - 2k_y^2 \bar{D} - \sigma g(0) + 2\sigma h(0)\bar{D}. \right]$$
(32)

For self-sustained detonations, since $(\bar{u} - \bar{D} \to 0)$ at the other end of the reaction region, $x \to -\infty$, the right-hand side of (24) must also vanish there as well. Using the fact that $\bar{u}' \to 0$ and $g(x) \to 0$ as $x \to -\infty$, we obtain the 'radiation' or Weyl-type boundary condition at the end of the reaction region

$$-\sigma u_1 - ik_v v_1 - h(x)\lambda_1/2 \rightarrow 0, x \rightarrow -\infty$$
 (33)

Faria et al¹ have detailed the solutions of the system (24)-(27) with boundary conditions (30) and (33) for the correct equilibrium profiles in Figure 1. In the next sub-section we introduce solutions of the same system for the box-shaped equilibrium profiles of Figure 2, compare them to the solutions in¹, and then proceed to the weakly nonlinear analysis and saturated states or cells resulting from the long-time or slow evolution of these linear solutions.

B. Linear solutions for Box Profile Equilibria

Next, we re-do the preceding linear stability analysis using the approximate box-shaped equilibrium profiles (11) and (12), and compare our results to those of the previous subsection. *Henceforth, we will refer to the regions to the right(left)*

of the discontinuity in $(\ref{eq:continuity})$ and $(\ref{eq:continuity})$ as the +(-) regions respectively, and attach +(-) subscripts to the solutions in each region.

As is standard in the method of normal modes⁸, we consider one arbitrary Fourier mode or wavenumber k_y in the y-direction, and subsequently focus on the most unstable k_y mode which first undergoes linear instability. For the boxprofiles of Figure 2, since all the equlibrium variables are constant on each side of the discontinuity, we may thus use a single normal or Fourier mode in x in each region. We therefore assume linear fields of the form

$$u_1(x, y, T_0, T_1, T_2) = u_{10}(T_1, T_2)e^{\sigma T_0 + ik_x x + ik_y y} + u_{10} * (T_1, T_2)e^{\sigma T_0 - ik_x x - ik_y y}$$
(34)

$$v_1(x, y, T_0, T_1, T_2) = v_{10}(T_1, T_2)e^{\sigma T_0 + ik_x x + ik_y y} + v_{10} * (T_1, T_2)e^{\sigma T_0 - ik_x x - ik_y y}$$
(35)

$$\lambda_{1}(x, y, T_{0}, T_{1}, T_{2}) = \lambda_{1}(T_{1}, T_{2}) e^{\sigma T_{0} + ik_{x}x + ik_{y}y} + \lambda_{10} * (T_{1}, T_{2}) e^{\sigma T_{0} - ik_{x}x - ik_{y}y}$$
(36)

where the * denotes a complex conjugate.

1. Solutions Behind the Shock

Using these, the $\mathcal{O}(\varepsilon)$, equations (A1) yield the linear dispersion relation to the right of the discontinuity in the equilibrium profiles, including just behind the shock at $x = 0^-$:

$$k_{x}\left(ik_{y}^{2}+k_{x}\sigma\right)+\bar{D}k_{x}^{2}\left(ik_{x}+e^{2\bar{D}q^{1/2}\theta}k(-1+q\theta)\right)$$

$$+1/2e^{2\bar{D}q^{1/2}\theta}k\left[2k_{y}^{2}(-1+q\theta)-k_{x}(k_{x}q^{1/2}\theta)+2i\sigma(-1+q\theta)\right]=0. \quad (37)$$

On the 'neutral curve' 1,8 where the temporal growth rate σ is zero, the *x* and *y*-wavenumbers k_x and k_y satisfy

$$k_x \left(ik_y^2 + k_x \sigma \right) + \bar{D}k_x^2 \left(ik_x + e^{2\bar{D}q^{1/2}\theta} k(-1 + q\theta) \right)$$

$$+ 1/2e^{2\bar{D}q^{1/2}\theta} k \left[2k_y^2 (-1 + q\theta) - k_x (k_x q^{1/2}\theta) \right] = 0.$$
 (38)

Since some coefficients of this cubic for the x-wavenumber k_x are imaginary, it is clear that we have two linear modes with complex x-wavenumbers which we denote as k_{x1+} and k_{x2+} for each value of the y-wavenumber k_y . In the context of hydrodynamic or hydromagnetic stability, this would be the setting of possible 'convective' instability, as opposed to 'temporal' instability where the growth rate σ has an imaginary part. Thus, adjacent to the neutral curve, weakly growing solutions

with $\sigma = 0^+ at x = 0^-$ just behind the shock take the form

$$\begin{split} \lambda_{1+}\left(x,y,T_{0},T_{1},T_{2}\right) &= \lambda_{10}\left(T_{1},T_{2}\right)e^{\sigma T_{0}+ik_{x_{1}+}+ik_{y}} + \\ \lambda_{10}*\left(T_{1},T_{2}\right)e^{\sigma T_{0}-ik_{x_{1}+}x-ik_{y}y} + \lambda_{20}\left(T_{1},T_{2}\right)e^{\sigma T_{0}+ik_{x_{2}+}+ik_{y}} + \\ \lambda_{20}*\left(T_{1},T_{2}\right)e^{\sigma T_{0}-ik_{x_{2}+}x-ik_{y}y} + \lambda_{30}\left(T_{1},T_{2}\right)e^{\sigma T_{0}+ik_{x_{3}+}+ik_{y}} + \\ \lambda_{30}*\left(T_{1},T_{2}\right)e^{\sigma T_{0}-ik_{x_{3}+}x-ik_{y}y}, \quad (39) \end{split}$$

with analogous expressions for the other linear fields u_1 and v_1 .

Note that k_x , the spatial wavenumber along the reaction channel being complex as noted above potentially allows for spatial growth of the linear modes, or so-called 'convective' instability³⁹. Since the linear modes in (34)-(36) are confined to the finite domain between x = 0 and $x = -x_{step}$, no blow-up of these linear fields occurs. We consider this later for specific parameter sets.

2. Solutions near the end of the Reaction Zone

To the left of the discontinuity or $x < -x_{step}$, the composite equation needs to be separately derived since $\lambda = 0$ and $\bar{u} = \bar{D}$ on that side. Using the first two $\mathcal{O}(\varepsilon)$ equations (A.1) yields the simpler composite equation

$$(\bar{D}^2 - 1)^{1/2} u_1'' + \sigma u_1' - k_y^2 u_1 = 0 \tag{40}$$

whose solutions may analogously be expressly as

$$\lambda_{1-}(x, y, T_0, T_1, T_2) = \lambda_{40}(T_1, T_2) e^{\sigma T_0 + ik_{x_1-}x + ik_y y} + \lambda_{40}*(T_1, T_2) e^{\sigma T_0 - ik_{x_1-}x - ik_y y} + \lambda_{50}(T_1, T_2) e^{\sigma T_0 - ik_{x_2-}x + ik_y y} + \lambda_{50}*(T_1, T_2) e^{\sigma T_0 - ik_{x_2-}x - ik_y y},$$
(41)

where

$$k_{x1-}/k_{x2-} = +/-ik_y/(\bar{D}^2 - 1)^{1/4}$$
 (42)

in the weakly nonlinear domain near the neutral curve $\sigma = 0$.

Note that one of our three wavenumbers is lost in our solution here due to the step discontinuity transition. It is straightforward to refine this by inserting a narrow boundary or inner solution in place of the step jump⁴⁰. However, as discussed below, our main focus will be nonlinear evolution of the solutions just behind the shock as considered in the previous subsection, and so we do not consider this here.

For each set of parameters k, \bar{D}, q, θ and k_y , the solution (39) and (41) on each side of the discontinuity may be directly derived. The boundary conditions (30) are then imposed on (39), and then this is matched to (41) by imposing the jump condition at the discontinuity obtained by integrating (29) across the discontinuity, i.e from $x = -x_{step}^-$ to $x = -x_{step}^+$. And finally the boundary condition (33) needs to be imposed on the solutions (41) to the left of the discontinuity.

Since our main focus will be on the nonlinear evolution of the linear solutions (39) and (41), we do not dwell too much on the details of this standard and straightforward procedure for step profiles in many areas of science⁴¹-⁴². However, for

the purposes of the nonlinear analysis in the following sections, as well as comparisons to the numerics on the nonlinear evolution of solutions in¹, we include below some typical linear solutions for parameter sets employed in the simulations in that paper.

In particular, we will find that the solutions (39) will be of primary interest to us in the formation and persistence of non-linear cellular patterns just behind the shock. Further behind the shock these cells decay away rapidly in space, and so one may position the discontinuity $x = -x_{step}$ appropriately and impose the discontinuity jump condition on the solutions (41) to the left of $-x_{step}$. The final step of enforcing the left boundary conditions (33) on the solutions (41) clearly requires the suppression of the unbounded k_{x1-} mode in (42).

However, as mentioned in the previous paragraph, we omit the details of this standard procedure for jump discontinuities, and focus primarily on the solutions (39) right behind the shock, and its nonlinear evolution. To this end, and for later reference in the results for the weakly nonlinear evolution, we list the wavenumbers in the solutions (39) for various parameter sets¹. For the first parameter set

$$\bar{D} = 1.05, q = 1.7, \theta = 1.65, k_v = \pi/5,$$
 (43)

the wavenumbers in (39) are

$$k_{x1+}/k_{x2+} = +/-0.484354 + 0.748685i, k_{x3+} = -0.782113i.$$
 (44)

For the second parameter set

$$\bar{D} = 1.05, q = 1.7, \theta = 1.65, k_v = 2\pi/13,$$
 (45)

the wavenumbers in (39) are

$$k_{x1+}/k_{x2+} = +/-0.392967 + 0.6656i, k_{x3+} = -0.615927i.$$
 (46)

For the third parameter set

$$\bar{D} = 1.05, q = 1.8, \theta = 1.65, k_v = 2\pi/13,$$
 (47)

the wavenumbers in (39) are

$$k_{x1+}/k_{x2+} = +/-0.3559 + 0.7859i, k_{x3+} = -0.6151i.$$
 (48)

And finally, for the fourth parameter set

$$\bar{D} = 1.05, q = 2.4, \theta = 1.389, k_v = 2\pi/15,$$
 (49)

the wavenumbers in (39) are

$$k_{x1+}/k_{x2+} = +/-0.1809 + 0.3503i, k_{x3+} = -0.4604i.$$
 (50)

VI. SECOND ORDER ANALYSIS

Having considered the linear perturbation equations, we proceed to the $O(\varepsilon^2)$ composite equation (18)-(20) for i=2, which is

$$L(\lambda_2) = \Gamma_2 \tag{51}$$

Since Γ_2 contains nearly two thousand terms, we evaluate it numerically for specific parameter sets using the individual second-order sources S_{21}, S_{22} and S_{23} in Appendix A. Suppressing the secular $e^{\sigma T_0 + ik_{x_1}x + ik_yy}$, $e^{\sigma T_0 + ik_{x_2}x + ik_yy}$ and $e^{\sigma T_0 + ik_{x_3}x + ik_yy}$ terms in Γ_2 requires

$$\frac{\partial \lambda_{i0}}{\partial T_1} = 0, i = 1, 2, 3 \tag{52}$$

Hence, as is often the case¹⁸, all the amplitudes in the linear solution (39) turn out to be unmodulated or constant on the first slow or long T_1 timescale.

Next, the second order particular solution of (51) may be computed using the method of undetermined coefficients as is standard (see¹⁸ for instance). Since it is exceptionally long, we display the typical harmonics in Appendix B, but omit the general coefficients which are extremely lengthy.

For any of our parameter sets (43)-(49) for instance, the second-order particular solution obtained by the classical method of undetermined coefficients simplifies after considerable computer algebra to lengthy expressions for λ_2 which are omitted for reasons of brevity. The particular solutions for the other two second-order fields u_2 and v_2 then follow from their expressions in terms of λ_2 in the paragraph preceding the composite equation (18) (used in the derivation of the equation).

These second-order solutions for the variables then feed into the third-order analysis which we consider next.

VII. THIRD-ORDER ANALYSIS AND NORMAL FORM

Finally, evaluating the third-order composite source Γ_3 from (10) for i = 3, and suppressing the secular terms as done at second order yields our final slow flow or normal form for the long(or slow)-time modulation of the amplitudes of the linear solutions or cells on the second slow T_2 timescale. Once again, the coefficients in these equations are too long to include in general and will only be presented for our various parameter sets. However, the general structure of these third-order slow flow or normal form equations is:

$$\frac{d\lambda_{10}}{dT_2} = \lambda_{10}(T_2) \left[c_1 + c_2 \lambda_{10}(T_2) \lambda_{10}^*(T_2) \right. \\
+ c_3 \lambda_{20}(T_2) \lambda_{20}^*(T_2) + c_4 \lambda_{30}(T_2) \lambda_{30}^*(T_2), \\
\frac{d\lambda_{20}}{dT_2} = \lambda_{10}(T_2) \left[c_1^* + c_2^* \lambda_{20}(T_2) \lambda_{20}^*(T_2) \right. \\
+ c_3^* \lambda_{10}(T_2) \lambda_{10}^*(T_2) + c_4^* \lambda_{30}(T_2) \lambda_{30}^*(T_2), \\
\frac{d\lambda_{30}}{dT_2} = \lambda_{30}(T_2) \left[d_1 + d_2 \lambda_{10}(T_2) \lambda_{10}^*(T_2) \right. \\
+ d_3 \lambda_{20}(T_2) \lambda_{20}^*(T_2) + d_4 \lambda_{30}(T_2) \lambda_{30}^*(T_2). \quad (53)$$

with coefficients for two of our three chosen parameter sets given in Appendix C.

VIII. ANALYSIS OF NORMAL FORM: THREE MODE SOLUTIONS

Writing the amplitudes and constants in the normal form (53) in polar form as

$$\lambda_{i0} = a_i Exp[ip_i], i = 1, 2, 3$$
 (54)

$$c_i = c_i Exp[it_i] = \beta_i + i\gamma_i, i = 1, 2, 3, 4$$
 (55)

$$d_i = d_i Exp[ir_i] = \delta_i + i\varepsilon_i, i = 1, 2, 3, 4$$
 (56)

and denoting the derivative with respect to T_2 by a prime, the normal form (53) equations separate into real and imaginary parts as:

$$a_{1}^{'} = a_{1}^{3}\beta_{2} + a_{1}\beta_{1} + a_{1}a_{2}^{2}\beta_{3} + a_{1}a_{3}^{2}\beta_{4}$$
 (57)

$$a_{2}' = a_{2}^{3}\beta_{2} + a_{2}\beta_{1} + a_{1}^{2}a_{2}\beta_{3} + a_{2}a_{3}^{2}\beta_{4}$$
 (58)

$$a_{3}' = a_{1}^{2}a_{3}\delta_{2} + a_{3}\delta_{1} + a_{2}^{2}a_{3}\delta_{3} + a_{3}^{3}\delta_{4}$$
 (59)

and

$$p_1' = a_1^2 \gamma_2 + \gamma_1 + a_2^2 \gamma_3 + a_2^3 \gamma_4 \tag{60}$$

$$p_{2}' = -a_{2}^{2} \gamma_{2} - \gamma_{1} - a_{1}^{2} \gamma_{3} - a_{3}^{2} \gamma_{4}$$
 (61)

$$p_{3}' = a_{1}^{2} \varepsilon_{2} + a_{3} \varepsilon_{1} + a_{2}^{2} \varepsilon_{3} + a_{3}^{3} \varepsilon_{4}$$
 (62)

The evolution of the amplitudes and phases of the linear solutions (39) on the second-order slow or long T_2 timescale is governed by equations (57)-(59), and (60)-(62) respectively. Considering the stable fixed points or equilibria of (57)-(59) OR (60)-(62) gives the possible asymptotic states to which the linear solutions (39) may settle. In the former case, the amplitudes a_i , i=1,...3 settle to constants while the phases ϕ_i , i=1,...3 are slowly modulated in the long-time solutions. In the latter case, the situation is exactly reversed, and slowly amplitude-modulated solutions result as asymptotic states.

A. Phase-Modulated Solutions

The non-trivial fixed points of (57)-(59) are given by linear equations for $z_i = a_i^2$, i = 1,...3 which may be easily obtained using Cramer's Rule. The characteristic equation for the Jacobian matrix at this fixed point is given by

$$\lambda^3 + b_1 \lambda^2 + b_2 \lambda + b_3 = 0, \tag{63}$$

where

$$b_{1} = -2\beta_{2} - \delta_{4},$$

$$b_{2} = \beta_{2}^{2} - \beta_{3}^{2} - \beta_{4}\delta_{2} - \beta_{5}\delta_{3} + 2\beta_{2}\delta_{4},$$

$$b_{3} = \beta_{2}\beta_{4}\delta_{2} - \beta_{3}\beta_{5}\delta_{2} - \beta_{3}\beta_{4}\delta_{3}$$

$$+ \beta_{2}\beta_{5}\delta_{3} - \beta_{2}^{2}\delta_{4} + \beta_{3}^{2}\delta_{4}$$
 (64)

The non-trivial fixed point $z_i = a_i^2$, i = 1,...,3 of (57)-(59) is stable if the Routh-Hurwitz conditions

$$b_1 > 0, b_3 > 0, b_1 b_2 - b_3 > 0$$
 (65)

are satisfied.

For the coefficients in (C1) for the parameters in (43), the fixed point $z_i = a_i^2, i = 1,...,3$ of (57)-(59) is

$$z_1 = 32.2607k_4, z_2 = 29.1465k_4, z_3 = -14.6542k_4$$
 (66)

with the stability conditions (65) simplifying to $b_1 = 5.12877 > 0$, $b_3 = -11.224 < 0$, and $b_1b_2 - b_3 = 20.4042 > 0$. Hence, there is no real fixed point corresponding to $z_i = a_i^2 > 0$, i = 1,...,3 for any k_4 value, and thus no three-mode solution corresponding to a stable fixed point of (57)-(59) to which the linear solutions (39) can settle for this parameter set.

For the coefficients in (C2) for the parameters in (49), the fixed point $z_i = a_i^2$, i = 1,...,3 of (57)-(59) is

$$z_1 = 35.2903k_4, z_2 = 35.2903k_4, z_3 = -6.11268k_4$$
 (67)

with the stability conditions (65) simplifying to $b_1 = 7.23104 > 0$, $b_3 = -219.647 < 0$, and $b_1b_2 - b_3 = -7.8368 < 0$. Once again, there is no real fixed point corresponding to $z_i = a_i^2 > 0$, i = 1, ..., 3 for any k_4 value, and thus no three-mode solution corresponding to a stable fixed point of (57)-(59) to which the linear solutions (39) can settle for this parameter set.

Hence, we turn next to briefly consider the theoretical analysis of amplitude-modulated solutions. although these will correspond to amplitudes growing linearly on the slow time, and so would not be relevant to the study of the numerically-observed spatial cells in¹.

B. Amplitude-Modulated Solutions

The non-trivial fixed points of (60)-(62) are also given by linear equations for $z_i = a_i^2$, i = 1,...3, and may be easily obtained using Cramer's Rule. The characteristic equation for the Jacobian matrix at this fixed point is given by

$$\lambda^{3} + b_{1}'\lambda^{2} + c_{2}'\lambda + c_{3}' = 0, \tag{68}$$

where

$$b'_{1} = -2\gamma_{2} - \varepsilon_{4},$$

$$b'_{2} = \gamma_{2}^{2} - \gamma_{3}^{2} - \gamma_{4}\varepsilon_{2} - \gamma_{5}\varepsilon_{3} + 2\gamma_{2}\varepsilon_{4},$$

$$b'_{3} = \gamma_{2}\gamma_{4}\varepsilon_{2} - \gamma_{3}\gamma_{5}\varepsilon_{2} - \gamma_{3}\gamma_{4}\varepsilon_{3}$$

$$+ \gamma_{2}\gamma_{5}\gamma_{3} - \gamma_{2}^{2}\varepsilon_{4} + \gamma_{3}^{2}\varepsilon_{4}$$
 (69)

The non-trivial fixed point $z_i = a_i^2, i = 1,...,3$ of (60)-(62) is stable if the Routh-Hurwitz conditions

$$b_{1}^{'} > 0, b_{3}^{'} > 0, b_{1}^{'} b_{2}^{'} - b_{3}^{'} > 0$$
 (70)

are satisfied.

Once again, as in the last subsection, it is straightforward to check that (60)-(62) have no real non-trivial fixed point for any of the sets of normal form coefficients (C1)-(C2) corresponding to the parameters in (43)-(49). Hence, there is no stable three-mode fixed point of (60)-(62) to which the linear solutions (39) can settle for any of our typical parameter sets.

In the next section, we consider two-mode solutions of the normal form, including real fixed points to which the linear field (39) may settle as a persistent cellular pattern behind the shock.

IX. ANALYSIS OF NORMAL FORM: TWO MODE SOLUTIONS

A. Phase-Modulated Solutions

The non-trivial fixed points of (57)-(59) corresponding to two non-trivial modes with $\lambda_{30} = 0$ are given by linear equations for $z_i = a_i^2$, i = 1, 2 with solutions

$$z_1 = -(\beta_1/(\beta_2 + \beta_3)), z_2 = -(\beta_1/(\beta_2 + \beta_3))$$
 (71)

The characteristic equation for the Jacobian matrix at this fixed point is given by

$$\beta_2^2 - \beta_3^2 - 2\beta_2 r + r^2 = 0 \tag{72}$$

Hence, it is stable for

$$\beta_2 < 0. \tag{73}$$

For the coefficients in (C1) corresponding to the parameters in (43), the two-mode fixed point $z_i = a_i^2, i = 1,...,3$ of (57)-(59) is

$$z_1 = a_1^2 = 36.2568k_4, z_2 = a_2^2 = 36.2568k_4, z_3 = 0,$$
 (74)

and it satisfies the stability condition (73). These may now be substituted into the right-hand sides of (60)-(62), which may then directly be integrated with respect to T_2 to obtain the phases p_1 and p_2 of the two modes.

Hence, the nonlinear evolution will lead to a two-mode solution corresponding to this stable fixed point of (57)-(59) to which the linear solutions (39) can settle for this parameter set. The resulting cellular patterns (39) are shown in Figures 2 and 3 at t=0 and t=1 to illustrate the very slow phase-modulation effect with time on the second T_2 timescale.

For the coefficients in (C2) (corresponding to parameters in (49)), the two-mode fixed point $z_i = a_i^2, i = 1,...,3$ of (57)-(59) is

$$z_1 = a_1^2 = 402.731k4, z_2 = a_2^2 402.731k4, z_3 = 0$$
 (75)

and it is also stable via condition (73). As before, these may now be substituted into the right-hand sides of (60)-(61), and these may then directly be integrated with respect to T_2 to obtain the phases p_1 and p_2 of the two modes.

The resulting cellular patterns are shown in Figures 5 and 6.

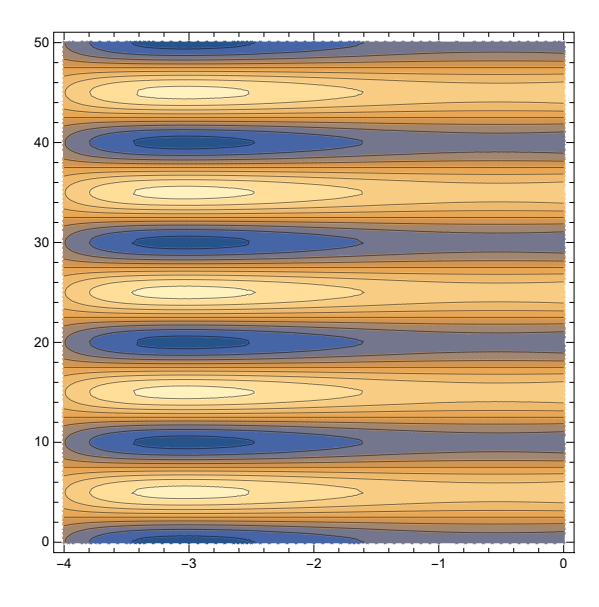


FIG. 3. Detonation cells behind the shock at x = 0 for the parameters in (43) at t = 0.

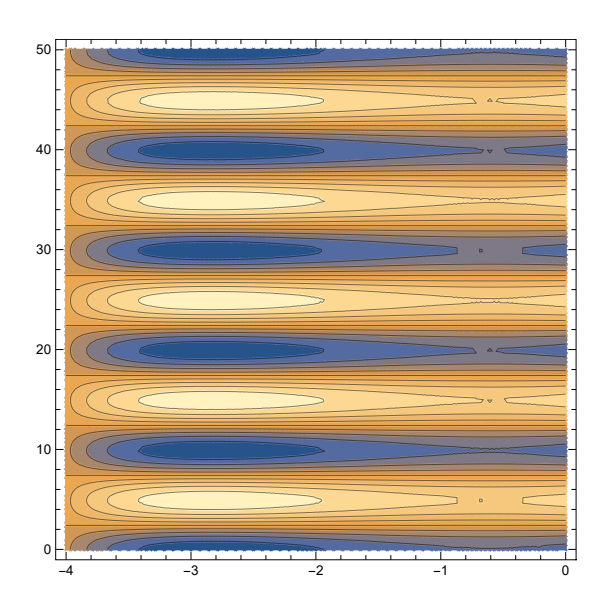


FIG. 4. Detonation cells behind the shock at x = 0 for the parameters in (43) at t = 1.

Comparing the stable persistent cellular patterns picked out in Figures 3 and 4 for the parameters in (43) to the numerical cells shown in Figure 5.5(c) of 1 , or in Figures 5 and 6 for parameters (49) with Figure 5.7(b) of 1 , the agreement is quite good. In particular, note that the cell shapes in Figures 5.5(c) and 5.7(b) of 1 are quite different for the two sets of parameters, and the shapes of the persistent patterns picked out by our nonlinear analysis in Figures 3/4 and 5/6 agree quite well with those numerically obtained cells. This includes cells which have vertical symmetry about the mid-point in both our Figures 3 and 4, as well as in the corresponding numerical cells computed in Figure 5.5(c) of 1 . Similar agreement is seen between the vertically asymmetric, elongated and slightly bent cell shapes for the parameter set (49) in our Figures 5 and

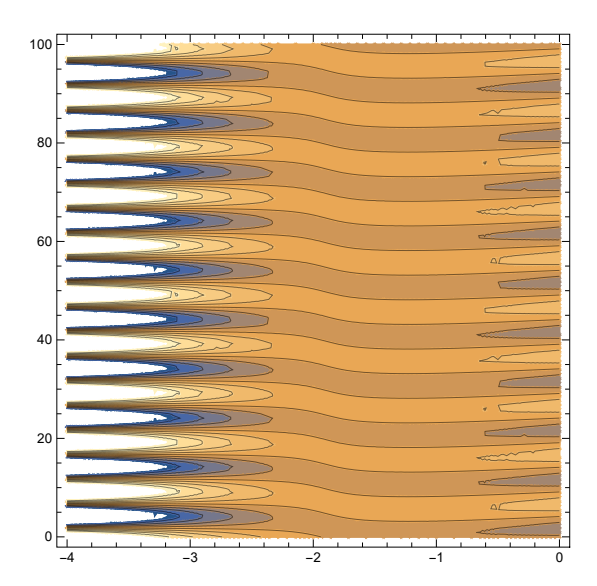


FIG. 5. Detonation cells behind the shock at x = 0 for the parameters in (49) at t = 0.

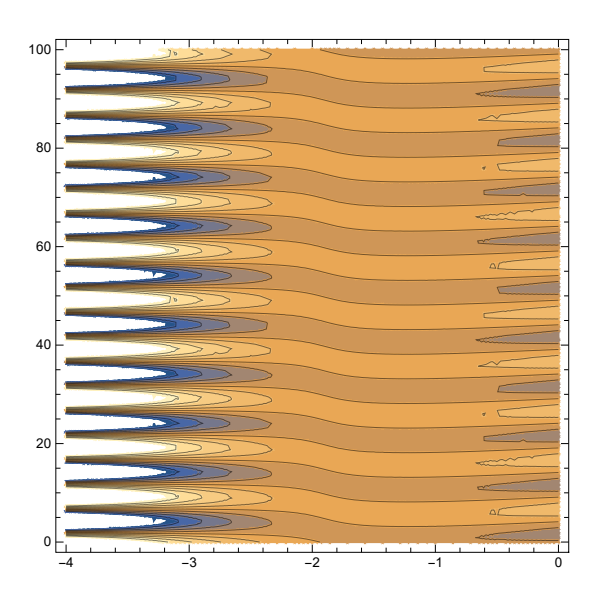


FIG. 6. Detonation cells behind the shock at x = 0 for the parameters in (49) at t = 1.

6, and Figure 5.7(b) of 1 . The same is true of the cell location. For (43), both the cells in our Figures 3 and 4, and in Figure 5.5(c) of 1 form right behind the shock. By contrast, for parameters (49), the cells form slightly behind the shock location.

The main discrepancy between our analytically predicted cells based on the simplified box-shaped equilibrium profiles and the corresponding numerical ones presented in is in their spatial wavelength k_x in the x-direction along the reaction channel. For parameters (43), the x-wavelength of the numerically computed cells in Figure 5.5(c) of is roughly $k_x = 0.7$, while our corresponding analytically derived cells in Figures 3 and 4 have $k_x = 2.15$. Similarly, for parameters (49), the x-wavelength of the numerically computed cells in Figure 5.5(c)

of¹ is roughly $k_x = 1.05$, while our corresponding analytically derived cells in Figures 3 and 4 have approximate wavenumber $k_x = 1.65$.

B. Amplitude Modulated Solutions

Stable two-mode amplitude modulated solutions with $a_3 = 0$ may also be directly obtained in a similar manner for all our parameter sets. However, these stable fixed points of (60)-(61), when substituted into (57)-(58) would result in mode amplitudes a_1 and a_2 which would grow linearly on the slow T_2 timescale, and thus not correspond to any stable patterns. Hence, we do not detail them here.

X. DISCUSSION AND CONCLUSIONS

In this paper, we have developed a nonlinear theory for the development and persistence of cellular patterns behind the shock front in self-sustained detonations using the significantly simplified detonation model developed in , where the analytical linear stability and numerical nonlinear results from that model were also extensively compared and found to have good agreement with those from the full reactive Euler equations.

For the purpose of analytical development of the nonlinear theory, we proceeded in the spirit of earlier investigations of a variety of hydrodynamic and hydromagnetic instabilities, such as the use of the so-called tangential discontinuity or vortex sheet step jumps in Kelvin-Helmholtz instabilities, or a box-shaped density profile in the analysis of crossed-field microwave sources. In that spirit, the actual numerically computed equilibrium profiles were replaced by box-shaped ones having a jump discontinuity. The discontinuity ensures transition to the correct values of the equilibrium variables at $x \to -\infty$, as well as allowing satisfaction of the boundary conditions (33) to give the correct linear eigenfunctions. However, its actual location does not affect our analysis of nonlinear two-dimensional cell formation behind that step jump.

As noted in the discussion following Figures 3 through 6, the agreement with the numerically-obtained results in 1 for the full nonlinear evolution is surprisingly good. In particular, both the shapes and dimensions of the persistent cells picked out by our nonlinear analysis agree quite well with those in 1 for the same set of parameters. The only significant difference or discrepancy from those numerical results is in the dimension or wavelength of the resulting cellular patterns in the x direction along the reaction channel.

As proved for instance for the compressible Kelvin-Helmholtz instability²⁹, the strongly nonlinear theory developed for the operating regimes of crossed-field magnetic devices^{31,32}, or edge density-related instabilities in tokamak plasmas³⁰, approximations of actual equilibrium profiles by step jump discontinuities, as done in this paper, work well for long-wavelength regimes. This is because the waves essentially do not register the spatial profile of the actual equilibria which occur on much shorter spatial scales. In regimes of

shorter wave operation, use of the accurate equilibrium profiles becomes much more important^{29,33,34}. Future work on this problem will be in that direction. In particular, it will involve the derivation of refined normal forms with coefficients which are integrals over the actual spatial equilibrium profiles (see³⁵ for example).

$$S_{1} = \left(-1 + \bar{D}^{2}\right) \left(-e^{\bar{D}\sqrt{q}\theta + \bar{D}^{2}q\theta}kk_{x_{1}}\frac{\partial\lambda_{10}}{\partial T_{1}} - k_{x_{1}}^{2}\frac{\partial\lambda_{10}}{\partial T_{1}}\right)$$

$$+i\bar{D}^{2}kk_{x_{1}}e^{\bar{D}\sqrt{q}\theta + \bar{D}^{2}q\theta}\frac{\partial\lambda_{10}}{\partial T_{1}} + \bar{D}^{2}k_{x_{1}}^{2}\frac{\partial\lambda_{10}}{\partial T_{1}}$$

$$+ie^{\bar{D}\sqrt{q}\theta + \bar{D}^{2}q\theta}kk_{x_{1}}q\theta\frac{\partial\lambda_{10}}{\partial T_{1}}$$

$$-2i\bar{D}^{2}e^{\bar{D}\sqrt{q}\theta + \bar{D}^{2}q\theta}kk_{x_{1}}q\theta\frac{\partial\lambda_{10}}{\partial T_{1}} + i\bar{D}^{4}e^{\bar{D}\sqrt{q}\theta + \bar{D}^{2}q\theta}kk_{x_{1}}q\theta\frac{\partial\lambda_{10}}{\partial T_{1}}\right)$$
(A1)

$$S_{2} = \left(-1 + \bar{D}^{2}\right) \left(-e^{\bar{D}\sqrt{q}\theta + \bar{D}^{2}q\theta}kk_{x2}\frac{\partial\lambda_{20}}{\partial T_{1}} - k_{x2}^{2}\frac{\partial\lambda_{20}}{\partial T_{1}}\right) + i\bar{D}^{2}kk_{x2}e^{\bar{D}\sqrt{q}\theta + \bar{D}^{2}q\theta}\frac{\partial\lambda_{20}}{\partial T_{1}} + \bar{D}^{2}k_{x2}^{2}\frac{\partial\lambda_{20}}{\partial T_{1}} + ie^{\bar{D}\sqrt{q}\theta + \bar{D}^{2}q\theta}kk_{x2}q\theta\frac{\partial\lambda_{20}}{\partial T_{1}} - 2i\bar{D}^{2}e^{\bar{D}\sqrt{q}\theta + \bar{D}^{2}q\theta}kk_{x2}q\theta\frac{\partial\lambda_{20}}{\partial T_{1}} + i\bar{D}^{4}e^{\bar{D}\sqrt{q}\theta + \bar{D}^{2}q\theta}kk_{x2}q\theta\frac{\partial\lambda_{20}}{\partial T_{1}} \right)$$

$$(A2)$$

Appendix A: Source Terms

The second-order sources are:

Appendix B: Second Order Particular Solutions

The second-order particular solutions of (51), after suppressing the secularities, take the following form in applying the method of undetermined coefficients:

$$\lambda_{2}(x,y,T_{o},T_{1},T_{2}) = \lambda_{2,1}e^{2\sigma T_{o} + (\bar{D}\sqrt{q} + \bar{D}^{2}q)\theta + 2ik_{x1}x + 2ik_{y}y} + \lambda_{2,1}^{*}e^{2\sigma T_{o} + (\bar{D}\sqrt{q} + \bar{D}^{2}q)\theta + 2ik_{x}^{*}x + 2ik_{y}y} + \lambda_{2,2}e^{2\sigma T_{o} + (\bar{D}\sqrt{q} + \bar{D}^{2}q)\theta + ik_{x1}x + ik_{x2}x + 2ik_{y}y} + \lambda_{2,3}e^{2\sigma T_{o} + (\bar{D}\sqrt{q} + \bar{D}^{2}q)\theta + ik_{x1}x + ik_{x2}x + 2ik_{y}y} + \lambda_{2,3}e^{2\sigma T_{o} + (\bar{D}\sqrt{q} + \bar{D}^{2}q)\theta + ik_{x1}x + ik_{x2}x + \lambda_{2,3}^{*}e^{2\sigma T_{o} + (\bar{D}\sqrt{q} + \bar{D}^{2}q)\theta + ik_{x1}x + ik_{x2}x + \lambda_{2,3}^{*}e^{2\sigma T_{o} + (\bar{D}\sqrt{q} + \bar{D}^{2}q)\theta + ik_{x1}x + 2ik_{y}y} + \lambda_{2,4}e^{2\sigma T_{o} + (\bar{D}\sqrt{q} + \bar{D}^{2}q)\theta + 2ik_{x2}x + 2ik_{y}y} + \lambda_{2,5}e^{2\sigma T_{o} + (\bar{D}\sqrt{q} + \bar{D}^{2}q)\theta + ik_{x1}x + 2ik_{y}y} + \lambda_{2,5}e^{2\sigma T_{o} + (\bar{D}\sqrt{q} + \bar{D}^{2}q)\theta + ik_{x1}x + 2ik_{y}y} + \lambda_{2,6}e^{2\sigma T_{o} + (\bar{D}\sqrt{q} + \bar{D}^{2}q)\theta + ik_{x1}x + \lambda_{2,6}^{*}e^{2\sigma T_{o} + (\bar{D}\sqrt{q} + \bar{D}^{2}q)\theta + ik_{x1}x + 2ik_{y}y} + \lambda_{2,6}e^{2\sigma T_{o} + (\bar{D}\sqrt{q} + \bar{D}^{2}q)\theta + ik_{x1}x + \lambda_{2,6}^{*}e^{2\sigma T_{o} + (\bar{D}\sqrt{q} + \bar{D}^{2}q)\theta + ik_{x1}x + \lambda_{2,6}^{*}e^{2\sigma T_{o} + (\bar{D}\sqrt{q} + \bar{D}^{2}q)\theta + ik_{x1}x + \lambda_{2,6}^{*}e^{2\sigma T_{o} + (\bar{D}\sqrt{q} + \bar{D}^{2}q)\theta + ik_{x1}x + \lambda_{2,6}^{*}e^{2\sigma T_{o} + (\bar{D}\sqrt{q} + \bar{D}^{2}q)\theta + ik_{x1}x + \lambda_{2,6}^{*}e^{2\sigma T_{o} + (\bar{D}\sqrt{q} + \bar{D}^{2}q)\theta + ik_{x1}x + \lambda_{2,6}^{*}e^{2\sigma T_{o} + (\bar{D}\sqrt{q} + \bar{D}^{2}q)\theta + ik_{x1}x + \lambda_{2,6}^{*}e^{2\sigma T_{o} + (\bar{D}\sqrt{q} + \bar{D}^{2}q)\theta + ik_{x1}x + \lambda_{2,6}^{*}e^{2\sigma T_{o} + (\bar{D}\sqrt{q} + \bar{D}^{2}q)\theta + ik_{x1}x + \lambda_{2,6}^{*}e^{2\sigma T_{o} + (\bar{D}\sqrt{q} + \bar{D}^{2}q)\theta + ik_{x1}x + \lambda_{2,8}^{*}e^{2\sigma T_{o} + (\bar{D}\sqrt{q} + \bar{D}^{2}q)\theta + ik_{x1}x + \lambda_{2,8}^{*}e^{2\sigma T_{o} + (\bar{D}\sqrt{q} + \bar{D}^{2}q)\theta + ik_{x1}x + \lambda_{2,1}^{*}e^{2\sigma T_{o} + (\bar{D}\sqrt{q} + \bar{D}^{2}q)\theta + ik_{x1}x + \lambda_{2,1}^{*}e^{2\sigma T_{o} + (\bar{D}\sqrt{q} + \bar{D}^{2}q)\theta + ik_{x1}x + \lambda_{2,1}^{*}e^{2\sigma T_{o} + (\bar{D}\sqrt{q} + \bar{D}^{2}q)\theta + ik_{x1}x + \lambda_{2,1}^{*}e^{2\sigma T_{o} + (\bar{D}\sqrt{q} + \bar{D}^{2}q)\theta + ik_{x1}x + \lambda_{2,1}^{*}e^{2\sigma T_{o} + (\bar{D}\sqrt{q} + \bar{D}^{2}q)\theta + ik_{x1}x + \lambda_{2,1}^{*}e^{2\sigma T_{o} + (\bar{D}\sqrt{q} + \bar{D}^{2}q)\theta + ik_{x1}^{*}x + \lambda_{2,1}^{*}e^{2\sigma T_{o} + ($$

$$u_2(x, y, T_o, T_1, T_2) = \frac{e^{-q\theta\lambda(x) - \sqrt{q}\theta\bar{u}(x)} \left(- e^{-q\theta\lambda(x) + \sqrt{q}\theta\bar{u}(x)} k(1 - q\theta + q\theta\bar{\lambda}(x)\lambda_2 - S_{23} + \frac{\partial\lambda_2}{\partial x}) \right)}{k\sqrt{q}\theta(-1 + \bar{\lambda}(x))}$$
(B2)

$$v_{2}(x, y, T_{o}, T_{1}, T_{2}) = \frac{e^{-q\theta\lambda(x) - \sqrt{q}\theta\bar{u}(x)}\left(-e^{-q\theta\lambda(x) + \sqrt{q}\theta\bar{u}(x)}k\left(1 - q\theta + q\theta\bar{\lambda}(x)\frac{\partial\lambda_{2}}{\partial x}\right)\right) - \frac{dS_{23}}{dy} + \frac{\partial^{2}\lambda_{2}}{\partial x\partial y}}{k\sqrt{q}\theta\left(-1 + \bar{\lambda}(x)\right)}$$
(B3)

Appendix C: Coefficients in Third-Ordel Normal Form (53)

For the parameter set (43), the coefficients in (53) are:

```
\begin{split} c_1 &= (-34.800907975220554 - 22.514089248191294i)k_4;\\ c_2 &= -(1.434565794129719 + 0.4371525972368321i);\\ c_3 &= (2.394424823144173 + 1.7845660726810215i);\\ c_4 &= -(0.7705499260252 - 1.0341564399245513i);\\ c_5 &= (0.043149805544178466 - 1.1704946669355656);\\ d_1 &= 36.3547447468111k_4;\\ d_2 &= -(1.36965135601604 + 0.9444635725621632i);\\ d_3 &= -(0.8674105661050214 - 1.0425095547332015i);\\ d_4 &= -2.2596338819071344 \quad \text{(C1)} \end{split}
```

For the parameter set (49), the corresponding coefficients in (53) are:

```
c_1 = (-81.39585230240318 + 42.03399851985379i)k_4;
c_2 = -(2.5215942414582306 - 3.6436687871361806i);
c_3 = (2.723675951041575 - 6.8362228067403485i);
c_4 = -(12.149223339495418 + 2.1519318977487902i);
c_5 = -(12.149223339495418 - 2.1519318977487902i);
d_1 = 106.97873365694113k_4;
d_2 = -(1.7051758449371195 - 1.5899717098177628i);
d_3 = -(1.7051758449371195 + 1.5899717098177628i);
d_4 = -2.187853835938873 (C2)
```

- ¹⁶L. Debnath and S. R. Choudhury, Nonlinear Instability Analysis (Advances in Fluid Mechanics), Computational Mechanics WIT Press (1997).
- ¹⁷P.G. Drazin and W.H. Reid, Hydrodynamic Stability, Cambridge Univ. Press (2004).
- ¹⁸R. K. Dodd, H. C. Morris, J. C. Eilbeck, J. D. Gibbon, Solitons and Non-linear Wave Equations, Academic Press (1984).
- ¹⁹M. Short and D. S. Stewart, Cellular Detonation Stability, J. Fluid Mech. 368, 229-262 (1998).
- ²⁰J. J. Erpenbeck, Nonlinear Theory of Unstable Two-Dimensional Detonation, Phys. Fluids 13, 2007-2026 (1970).
- ²¹A. Majda and V. Roytburd, Low-frequency multidimensional instabilities for reacting shock waves, Stud. Appl. Math, 87 135-174 (1992).
- ²²J. Yao and J. Stewart, On the dynamics of multi-dimensional detonation, J. Fluid Mech. 309, 225-275 (1996).
- Lind Mech. 309, 223-273 (1990).
 D. S. Stewart, T. D. Aslam, and J. Yao, On the evolution of cellular detonation, Proc. Combust. Inst. 26, 2981–2989 (1996).
- ²⁴A. Majda and E. Thomann, Multi-dimensional shock fronts for second order wave equations, Commun. Partial Diff. Equations 12, 777-828 (1987).
- ²⁵R. R. Rosales and A. J. Majda, Weakly nonlinear detonation waves, SIAM J. Appl. Math 43, 1086–1118 (1983).
- ²⁶A. Majda, A qualitative model for dynamic combustion. SIAM J. Appl. Math 41, 70–93 (1980).
- ²⁷B. V. Voitsekhovskii, V. V. Mitrofanov, and M. Y. Topchian, The Structure of Detonation Front in Gases, Report FTD-MTD-64-527, Foreign Technology Division, Wright Patterson Air Force Base, OH, 633-821 (1966).
- ²⁸R. R. Rosales, Diffraction effects in weakly nonlinear detonation waves, Nonlinear Hyperbolic Problems, Springer 27–239 (1989).
- ²⁹S. Roy Choudhury and R.V.E. Lovelace, On the Kelvin-Helmhotz Instabilities of High-Velocity Magnetized Shear Layers, Astrophys. J. 302 188-199 (1986); S. Roy Choudhury, Kelvin-Helmholtz instabilities of supersonic, magnetized shear layers, J. Plasma Phys. 35, 375-392 (1986).
- ³⁰S. Roy Choudhury and P.K. Kaw. Ionization and edge-density gradient effects on MARFE instabilities in tokamak plasmas, Phys. Fluids B: Plasma Phys. 1, 1646-1653 (1989).
- ³¹D. J. Kaup, S. Roy Choudhury, and G. E. Thomas, Full second-order cold-fluid theory of the diocotron and magnetron resonances, Phys. Rev. A. 38, 1402 (1988).
- ³²D. J. Kaup, P. J. Hansen, and S. Roy Choudhury, Linear stability analysis of the Vlasov–Poisson equations in high density plasmas in the presence of crossed fields and density gradients, Phys. Fluids. 29, 4047-4054 (1986).
- ³³D. J. Kaup, Initiation and Stationary Operating States in a Crossed-Field Vacuum Electron Device, Intense Microwave Pulses IX, Proceedings of SPIE 4720, 67-74 (2002).
- ³⁴D. Kaup and G. E. Thomas, Stationary operating density profiles in a crossed field amplifier, J Plasma Phys. 59, 259-276 (1998).
- ³⁵D. J. Kaup and G. E. Thomas. The Third-Order Singular-Perturbation Expansion of the Planar Cold-Fluid Magnetron Equations, Stud. Appl. Math. 81, 57-78 (1989).
- ³⁶S. Roy Choudhury, The initial-value problem for the Kelvin-Helmholtz instabilities of high-velocity and magnetized shear layers, Q. Appl. Math. 54, 637-662 (1996).
- ³⁷S. Roy Choudhury, K. G. Brown, Quasiperiodicity and chaos in the nonlinear evolution of the Kelvin-Helmholtz instability of supersonic anisotropic tangential velocity discontinuities, Q. Appl. Math. 61, 41-71 (2003).
- ³⁸S. Roy Choudhury, Nonlinear Evolution of the Kelvin–Helmholtz Instability of Supersonic Tangential Velocity Discontinuities, J. Math. Anal. Appl. 214, 561-586 (1997).
- ³⁹G. Schmidt, Physics of High Temperature Plasmas, Academic Press (1979).
 ⁴⁰S. Roy Choudhury, Global Asymptotic Analysis of the Kelvin-Helmholtz
- Instabilities of Supersonic Shear Layers, Can. J. Phy. 68, 334-340 (1990). ⁴¹C. M. Bender and S. A. Orszag, Advanced Mathematical Methods for
- Scientists and Engineers I: Asymptotic methods and perturbation theory, Springer (1999).
- ⁴²G. Arfken, H. Weber, and F. Harris, Mathematical Methods for Physicists, Elsevier (2012).

¹L. M. Faria, A. R. Kasimov, and R. R. Rosales, Theory of weakly nonlinear self-sustained detonations, J. Fluid Mech. 784, 163-198 (2015).

²W. Fickett and W. C. Davis, Detonation: theory and experiment (2000).

³J. H. S. Lee, The Detonation Phenomenon, Cambridge University Press (2008).

⁴L. Landau and E. M. Lifschitz, Fluid Mechanics, Pergamon Press (1959).

⁵J. J. Erpenbeck, Stability of idealized one-reaction detonations, Phys. Fluids 7, 684-696 (1964).

⁶P. Clavin and F. A. Williams, Analytical studies of the dynamics of gaseous detonations, Philos. Trans. R. Soc. A 370, 597–624 (2012).

⁷H. I. Lee and D. S. Stewart, Calculation of linear detonation instability: One-dimensional instability of plane detonation. J. Fluid Mech. 212, 103–132 (1990).

⁸S. Chandrasekhar, Hydrodynamic and Hydromagnetic Stability, Dover (1981).

⁹M. Short and D. S. Stewart, Cellular Detonation Stability Part 1. A normal-mode linear analysis, J. Fluid Mech. 368, 229–262 (1998).

¹⁰I. Brailovsky, M. Frankel, and G. I. Sivashinsky, Galloping and Spinning Modes of Subsonic Detonation, Combust. Theor. Model. 4, 47-60 (2000).

¹¹G. I. Sivashinsky, On Spinning Propagation of Combustion Waves, SIAM J. Appl. Math 40, 432-438 (1981).

¹²M. Short and D. S. Stewart, Low-frequency two-dimensional linear instability of plane detonation, J Fluid Mech. 340, 249-295 (1997).

 ¹³M. Short, Multidimensional Linear Stability of a Detonation at High Activation Energy, SIAM J. Appl. Math 57, 307-326 (1997).

¹⁴B. D. Taylor, A. R. Kasimov, and D. S. Stewart, Mode selection in weakly unstable two-dimensional detonations, Combust. Theory Model. 13, 973–992 (2009).

¹⁵D. J. Wollkind, V. S. Manoranjan and L. Zhang, Weakly Nonlinear Stability Analysis of Prototype Reaction-Diffusion Model Equations, SIAM Review 36, 176-214, (1994).